substitute for our 'aberration function'; this monochromator function would describe the intensity passed by the monochromator as a function of wavelength, including 'band-pass' limits at the two ends and could thus have the effect both of altering the effective $K\alpha_2$ to $K\alpha_1$ intensity ratio and of adding a white-radiation component that is so clearly needed.

We emphasize that all our experiments have been made at low temperature (20 K or less) and we have assumed thermal diffuse scattering to be negligible. At higher temperatures, TDS becomes appreciable, perhaps being as large as, and in the opposite sense from, truncation losses. Conceivably, then, one could end up worse off by correcting room-temperature data for truncation while ignoring TDS. But our work on truncation is based on the fact that, for careful work in such areas as electron-distribution studies and highly precise bond-length determinations, low-temperature data are of utmost importance (particularly for molecular crystals), not only to avoid TDS but also to permit the accurate determination of the displacement parameters U_{ij} that is afforded by high-angle intensity data. For such experiments, truncation losses are extremely important: an intensity loss of 15% at $2\theta = 40°$ for Mo radiation corresponds to an apparent increase in the isotropic component of the atomic displacement coefficient U of over 0.004 Å^2. Further efforts to arrive at convenient and reliable methods of correcting for such losses are clearly warranted.

Afterword

At the suggestions of thoughtful referees, we add a few comments.

(1) We emphasize that the 'basic profile' depends on the characteristics (size, mosaic character, *etc.*) of the particular crystal being studied; it would be dangerous and unjustified to use the basic profile for one crystal in analyzing the high-angle profiles of another.

(2) Our recommendations for low-temperature measurements apply to molecular crystals. For many inorganic systems with high Debye temperatures, measurements at or near room temperature might well be adequate.

(3) Our experimental data were, as we have noted, obtained with the monochromator in the perpendicular orientation. For instruments with a parallel configuration, expressions for the spectral resolution would need to be modified.

(4) An interesting experiment, which we have not carried out, would be to measure the band-pass characteristics of the monochromator, perhaps (as suggested by Mathieson, 1989*a*) by scanning the profile using a very narrow slit.

(5) We regard this work as developmental; while RD has devised many computer programs to carry out the various calculations, these programs are being continuously revised and have not been thoroughly debugged. Thus, they are not available for distribution.

We are indeed indebted to Professor A. McL. Mathieson for many helpful and insightful comments.

References

ALEXANDER, K. E. & SMITH, G. S. (1962). *Acta Cryst.* **15**, 983-1004.
BEARDEN, J. A. (1967). *Rev. Mod. Phys.* **39**, 78-124.
COMPTON, A. H. & ALLISON, K. S. (1935). *X-rays in Theory and Experiment*, pp. 640, 745. New York: Van Nostrand.
DESTRO, R. (1988). *Aust. J. Phys.* **41**, 503-510.
DESTRO, R. & MARSH, R. E. (1987). *Acta Cryst.* A**43**, 711-718.
HOYT, A. (1932). *Phys. Rev.* **40**, 477-483.
LADELL, J. & SPIELBERG, N. (1966). *Acta Cryst.* **21**, 561-567.
MATHIESON, A. McL. (1968). *Rev. Sci. Instrum.* **39**, 1834-1837.
MATHIESON, A. McL. (1982). *Acta Cryst.* A**38**, 378-387.
MATHIESON, A. McL. (1989*a*). *Acta Cryst.* A**45**, 613-620.
MATHIESON, A. McL. (1989*b*). Private communication.
SAMSON, S., GOLDISH, E. & DICK, C. J. (1980). *J. Appl. Cryst.* **13**, 425-432.
STOKES, A. R. (1948). *Proc. Phys. Soc. London Sect. A*, **61**, 382-391.

Acta Cryst. (1993). A**49**, 190-198

Energy-Dispersive Diffuse X-ray Scattering Technique. I. Principles

BY JOHN S. REID

Department of Engineering, Fraser Noble Building, The University, Aberdeen AB9 2UE, Scotland

(*Received* 23 *May* 1992; *accepted* 7 *August* 1992)

Abstract

Energy-dispersive diffuse X-ray scattering is a particularly appropriate technique for use with high-energy synchrotron-radiation sources. Its multiplex and geometric advantages are outlined and the comparatively simple principles behind the technique are detailed. The energy-dispersive scan spreads scatter-

0108-7673/93/010190-09$06.00

ing in reciprocal space along radial lines, with equal-energy steps corresponding to equal-scattering-vector steps. In a typical experimental configuration, the resolution function of the apparatus is substantially lozenge shaped in reciprocal space: modest resolution is obtained along radial lines whereas good resolution can be obtained in transverse directions if the limiting geometrical factors are kept narrow. The factors influencing the conversion of the observed scan intensities to absolute units are discussed and methods given of minimizing the difficulties. Paper II of this series will discuss the application of these methods, notably to measurements of silicon.

Introduction

Diffuse X-ray scattering studies are to be found in recent literature on a wide range of materials and for an equally wide range of purposes. Extended discussions can be found, for example, in articles by Schultz (1982) on applications to materials science, Welberry (1985) and Jagodzinski (1987) on disorder scattering and Lal (1989) on point-defect aggregates in single crystals. In addition, many articles cover specific diffuse-scattering measurements on low-dimensional structures, superionic conductors, superconductors, organic crystals and other systems. Nonetheless, the experimental determination of diffuse X-ray scattering has been hampered by two features of the phenomenon: its weakness and the necessity to measure diffuse scattering over an extended region of reciprocal space to determine its structure. Experiments are notoriously time consuming and difficult to calibrate. Several approaches to these difficulties promise to reduce them substantially. Increasing the incident flux in a traditional monochromatic-scattering apparatus by operating the scattering experiment close to a synchrotron-radiation source has been shown to be effective under favourable conditions (Matsubara & Georgopoulos, 1985; Iwasaki *et al.*, 1989). For more general use, it is highly desirable to employ experimental techniques with some multiplex advantage. (The term *multiplex* is used here in its spectroscopic sense, implying a simultaneous recording of all the resolution elements and, usually, subsequent processing to extract the desired information.)

A variety of position-sensitive detectors have been developed to allow an extended arc in reciprocal space to be sampled during a single measurement (Hashegawa *et al.*, 1986). Maeta *et al.* (1988) report diffuse-scattering measurements made with a single setting of such a detector, while Osborn & Welberry (1990) describe the technique in some detail. Area detectors in the form of CCDs, high-pressure proportional counters and photoluminescent image plates have developed considerably over the past few years. Although all have coarse spatial resolution in comparison with the best photographic film, the image plate in particular has now developed to offer a much wider dynamic range than conventional film and an improvement in photon sensitivity by about two orders of magnitude. Iwasaki, Matsuo, Ohshima & Hashimoto (1990) reported one of the first diffuse-scattering studies using such a device. In this paper a third multiplex method is outlined, using the Laue geometry of fixed detector and fixed crystal illuminated by a broad-band X-ray beam.

In this method, the diffuse scattering is displayed on an energy-dispersive detector whose spectrum directly maps a line of scattering vectors, as shown in Fig. 1 and explained fully in the next section. The principle was first exploited by Harada, Iwata & Ohshima (1984) using white radiation from a rotating-anode source but it is most appropriately developed in the context of a synchrotron-radiation source. The counting advantage over a monochromatic experiment is twofold. Firstly, an entire scan is

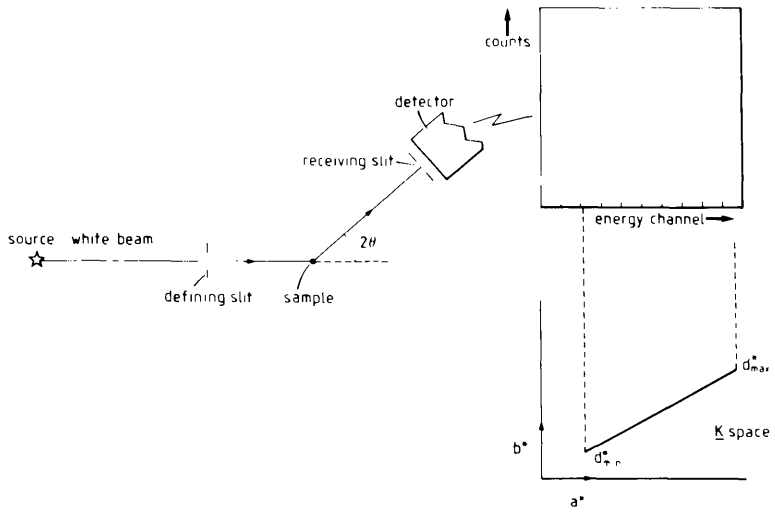

Fig. 1. Schematic diagram of the energy-dispersive diffuse X-ray scattering technique. The energy spectrum maps onto the scattering from a radial line of scattering vectors **K** of length from d^*_{min} to d^*_{max} determined by sin θ.

collected at once (the multiplex advantage). Secondly, the energy resolution of a solid-state energy-dispersive detector has a bandpass that is typically 100 times greater than the bandpass of a single-crystal mosaic monochromator. Hence, a much larger fraction of the incident-beam spectral distribution contributes to the scattering in each counting channel than in a monochromatic experiment. The energy bandpass is in fact much better matched to the geometric contributions to the resolution of a typical scattering experiment than is the case with a crystal monochromator.

Some other advantages of the technique are that it needs only comparatively simple and correspondingly less-expensive station apparatus; it allows a reduction in observing time or, alternatively, the use of samples too small to contemplate by traditional means; operationally, Laue geometry is easier to set up and maintain on a diffractometer than monochromatic geometry. The energy-dispersive scan covers a straight line of scattering vectors in reciprocal space, in contrast to the curved lines scanned by position-sensitive methods. A whole plane of reciprocal space may be scanned simply by a scattered beam emerging through a single hole in the sample chamber, provided only that the sample can be rotated independently about the main diffractometer axis. This has potential advantages for measurements at high pressure, variable temperature or other specialized sample environments. Two or more energy-dispersive detectors recording simultaneously at different 2θ will allow a scattering plane to be scanned at coarse and fine resolution simultaneously. Alternatively, there is the possibility of having a range of out-of-plane counters detecting simultaneously, such as have been employed on neutron time-of-flight apparatus. Most of these possibilities remain to be explored.

In the following sections, the principles of the technique are laid out and in paper II an application is made to a determination of the thermal diffuse scattering from silicon.

Principles of the technique

The spatial Laue scattering pattern, which is that recorded photographically, is the pattern given by a single mirror reflection of the incident X-ray beam from each crystal plane. As with a system of mirrors, if the crystal is rotated the pattern of Laue spots rotates in the same direction at twice the speed. To appreciate the diffuse scattering observed within the apparently fixed geometrical form of the Laue pattern, attention must be paid to the other dimension of the pattern, its energy. A given index of Laue spot has its highest energy when the spot is closest to the straight-through direction (smallest 2θ); the spot slides down the energy scale as it rotates towards the back-reflection direction. Indeed, the spot will fade out if the energy required is below the smallest photon energy available in the incident beam.

For any fixed position of the crystal, the detector records scattering with scattering vectors along a radial line in reciprocal space, each scattering vector contributed by a different incident and scattered energy. An energy-dispersive detector therefore separates each scattering vector along this radial line, within the limits of its energy resolution. For example, Laue spots that correspond to superimposed Bragg reflections are separated by an energy-dispersive detector into a spectrum of equally spaced lines corresponding to the Bragg reflections, with the diffuse scattering along the same radial direction in reciprocal space appearing between these lines. Once the Laue pattern is seen in energy space as well as reciprocal space, the diffuse-scattering component becomes simpler to visualize.

Indeed, the scope and limitations of recording diffuse scattering can be deduced directly from first principles. Let $\mathbf{K}$ be the scattering vector for a fixed counter (2θ) and fixed crystal. In terms of incident and scattered wave vectors,

$$\mathbf{K} = \mathbf{k}' - \mathbf{k}_0. \tag{1}$$

In a notation similar to that used in *International Tables for X-ray Crystallography* (1983),

$$\mathbf{K} = h\mathbf{a}^* + k\mathbf{b}^* + l\mathbf{c}^* = \mathbf{H} \cdot \mathbf{A}^*, \tag{2}$$

where

$$\mathbf{H} = (h\ k\ l). \tag{3}$$

In general, h, k, l are noninteger and

$$\mathbf{A}^* = \begin{pmatrix} \mathbf{a}^* \\ \mathbf{b}^* \\ \mathbf{c}^* \end{pmatrix} \tag{4}$$

defines the unit vector in reciprocal space with

$$\mathbf{a}^* = 2\pi \mathbf{b} \times \mathbf{c} / V, \tag{5}$$

where V is the volume of the real unit cell whose unit vectors are $\mathbf{a}$, $\mathbf{b}$, $\mathbf{c}$; similarly for $\mathbf{b}^*$ and $\mathbf{c}^*$. The distinction between $\mathbf{K}$, measured in Å $^{-1}$, and $\mathbf{H}$, a measure in terms of the reciprocal-cell dimensions, is important.

The length of $\mathbf{K}$, which determines the wavelength of the Laue scattering, is given through the reciprocal-space metric $\mathbf{G}^{-1}$

$$\mathbf{G}^{-1} = \begin{pmatrix} (a^*)^2 & a^*b^* \cos\gamma^* & a^*c^* \cos\beta^* \\ a^*b^* \cos\gamma^* & (b^*)^2 & b^*c^* \cos\alpha^* \\ a^*c^* \cos\beta^* & b^*c^* \cos\alpha^* & (c^*)^2 \end{pmatrix} \tag{6}$$

as d^*, where

$$|\mathbf{K}|^2 = (d^*)^2 = \mathbf{H}\mathbf{G}^{-1}\mathbf{H}'. \tag{7}$$

For a cubic crystal with a as the cubic-lattice constant, this reduces to

$$d^* = 2\pi|\mathbf{H}|/a. \quad (8)$$

The wavelength, λ, and hence the energy, for any scattering vector is found through Bragg's law,

$$\lambda = 2d_{\mathbf{K}} \sin\theta, \quad (9)$$

where

$$d_{\mathbf{K}} = 2\pi/d^*.$$

Equivalently,

$$d^* = 4\pi(\sin\theta)/\lambda, \quad (10)$$

with d^* being determined from (7). For a cubic crystal,

$$d_{\mathbf{K}} = a/|\mathbf{H}|, \quad (11)$$

whence (9) becomes the familiar

$$2a \sin\theta = |\mathbf{H}|\lambda. \quad (12)$$

For a given wavelength range, from λ_{min} to λ_{max}, the range of reciprocal space in $Å^{-1}$ seen by a fixed energy-dispersive detector is from d^*_{min} to d^*_{max} where

$$d^*_{min} = 4\pi(\sin\theta)/\lambda_{max}, \quad d^*_{max} = 4\pi(\sin\theta)/\lambda_{min}, \quad (13)$$

hence the range, d^*_{range}, is

$$d^*_{range} = 1.01355(E_{max} - E_{min}) \sin\theta, \quad (14)$$

where the corresponding photon energies are expressed in keV. For a cubic crystal,

$$|\mathbf{H}|_{range} = 2a(\sin\theta)(1/\lambda_{min} - 1/\lambda_{max}). \quad (15)$$

It follows from these equations that, for a detector of fixed energy spread, the range of $|\mathbf{K}|$ scanned increases with $\sin\theta$; the minimum value of $|\mathbf{K}|$ also increases with $\sin\theta$. Equal steps in energy, ΔE, cover equal lengths in reciprocal space Δd^*, where the steps again depend on $\sin\theta$:

$$\Delta d^* = 1.01355\Delta E \sin\theta \quad (16)$$

(ΔE in keV). The obvious strategy for measuring diffuse scattering in Laue geometry is therefore to fix 2θ such that the energy range of the detector covers an appropriate range in reciprocal space. The crystal is then rotated so that successive radial lines in reciprocal space are recorded by the detector. If the ω axis alone is turned (the axis parallel to the principal axis of the diffractometer) then a fan of radial lines in the scattering plane will be sampled. The inherent restriction of the scan to *radial* lines in reciprocal space is a significant difference between the Laue scan and a position-sensitive detector or a neutron time-of-flight scan, where the orientation of the scan depends on 2θ.

The method will fail to record weak diffuse scattering if a Laue spot enters the counter for a chosen crystal orientation, due to saturation of the counter by the Laue intensity. In general there is a Laue spot in every direction in reciprocal space, if one considers a high enough reflection index. However, for materials with a small unit cell, the energy associated with high-index Laue spots is correspondingly high, from (7) and (9), and for most of these spots is outside the range of incident-beam energy and detector response. Nonetheless, their potential presence shows that a rapid high-energy fall-off in the incident-beam spectrum and in the detector response is advantageous. The Debye-Waller factor and the general decrease in scattering factors also helps to reduce the intensity of unwanted high-index scattering.

Viewed alternatively, the Ewald sphere is the contour of scattering vectors sampled at constant diffraction energy. Hence a material with a large unit cell has as many Laue spots within this contour as a small unit cell would show for radiation of a correspondingly higher energy. In both cases (14) suggests that the same method is used to produce a smaller d^* range (removing unwanted high-index spots), namely to scan the given range of $\mathbf{H}$ by choosing a small value of 2θ.

Resolution limitation

The resolution limitation of a technique is an important consideration for diffuse-scattering experiments, particularly in relation to how close one can approach a Bragg reflection. The resolution of the Laue technique in the radial direction in reciprocal space is at least the energy resolution of the detector, through (16). Fig. 2(a) illustrates the corresponding geometry. If $\Delta E = 0.125$ keV HWHM (half-width at half-maximum), as typically may be the case at lower energies for a high-purity Ge or Si(Li) detector, and $2\theta = 30°$, then the half-width $\Delta d^* = 0.033$ $Å^{-1}$. (For the lowest energies the resolution is better.) As a

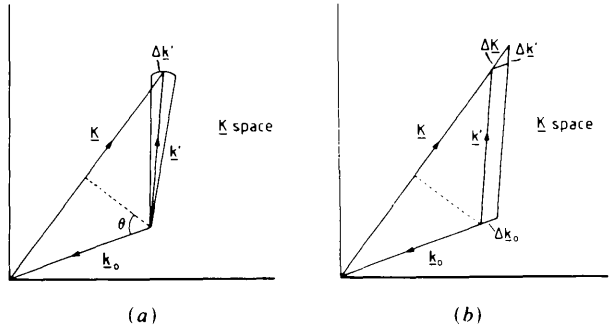

Fig. 2. (a) The finite size of the sample and detector both contribute a spread $\Delta\mathbf{k}'$ of scattered wave vectors. The corresponding spread of scattering vectors $\Delta\mathbf{K}$ is $\Delta k' \cos\theta$ parallel to $\mathbf{K}$ and $\Delta k' \sin\theta$ perpendicular to $\mathbf{K}$. (b) The finite energy resolution of the detector gives rise to a spread of scattering vectors $\Delta\mathbf{K}$ that is parallel to $\mathbf{K}$.

function of energy, the half-width at half-maximum energy resolution of the Gaussian peak of an energy-dispersive detector, $\Delta_{HWHM}(E)$ in keV, is given by the expression

$$\Delta^2_{HWHM}(E) = \Delta^2_{el} + kE, \qquad (17)$$

where Δ_{el} and k are constants (see, for example, Krumrey, Tegeler & Ulm, 1989). Typically, $\Delta_{el} = 0.060$ keV and $k = 0.001$ keV, giving an increase in Δd^* to 0.044 Å^{-1} at about 25 keV.

If one is interested in scattering that is located in a well defined region of reciprocal space, the strategy that maximizes the resolution in this region (*i.e.* minimizes Δd^*) is to move the scattering to the largest practicable energy. This is simply achieved by reducing 2θ appropriately.

The geometrical contribution to the resolution is likely to be dominated by the finite sizes of the sample and of the detector slit, the spread in incident-beam directions being comparatively negligible. These sizes both contribute to a spread in scattered wave vectors $\Delta\mathbf{k}'$ perpendicular to $\mathbf{k}'$ and hence a spread of scattering vectors $\Delta\mathbf{K}$ with an orientation depending on θ, as shown in Fig. 2(*b*). For small θ this spread is almost entirely radial, the transverse component being $\Delta\mathbf{k}' \sin\theta$. For example, if detector and sample are both 1 mm wide and separated by 300 mm, for $2\theta = 30°$ and a wavelength of 1 Å the transverse half-width resolution is 0.0054 Å^{-1}, a usefully small figure. Achievable reductions in 2θ, detector and sample sizes could improve the resolution to 0.001 Å^{-1}, though with an increase in practical problems.

For the example values above, the geometrical contribution to the *radial* half-width resolution is 0.021 Å^{-1}, significantly less than the energy-spread contribution. It is typical of this Laue technique that the overall resolution function can be strongly lozenge shaped, allowing a fine resolution in azimuthal directions in reciprocal space and modest resolution in radial directions. The fine resolution can be degraded by the mosaic spread of the sample, which contributes a spreading purely transverse to the scattering vector $\mathbf{K}$. To put this in perspective, 4′ of mosaic spread results in a spread $\Delta\mathbf{K}$ of $1.16 \times 10^{-3}\, d^*$.

Conversion of measurements to absolute units

If a counter observes a (dead-time corrected) flux of $J_{obs}(\mathbf{K})$, in photons s^{-1}, then the corresponding scattering cross section $I_{exp}(\mathbf{K})$, in electron units/cell, is given by

$$I_{exp}(\mathbf{K}) = J_{obs}(\mathbf{K}) A(\theta, \varphi, \chi, \omega, \lambda) \sigma_t (1 + D) / J_{in}(\lambda) \varepsilon(\lambda), \qquad (18)$$

where $A(\theta, \varphi, \chi, \omega, \lambda)$ is the absorption-related factor, dependent on the detector angle 2θ, the crystal orientation angles (φ, χ, ω) and the wavelength, λ. σ_t is the Thomson scattering cross section, given by

$$\sigma_t = A_d (1 + k_p \cos^2 2\theta) \lambda_c^2 / R^2 (1 + k_p),$$

where A_d is the area of the detector; k_p is the polarization fraction in the scattering plane; λ_c is the Compton wavelength of an electron, namely 3.86159×10^{-13} m; R is the sample-to-detector distance. D is the apparatus-resolution correction, sometimes called the divergence correction, which is a measure of a systematic shift introduced by finite incident- and scattered-beam cross fire, finite counter resolution and finite sample mosaic spread. It depends on $\mathbf{K}$, λ and the scattering geometry. With sympathetic apparatus design it is small. $J_{in}(\lambda)$ is the flux delivered through the incident-beam-defining aperture by the (synchrotron) source. $\varepsilon(\lambda)$ is an efficiency function, including the efficiency of the detector and absorption of air and windows, particularly at longer wavelengths.

Complete conversion is achieved by evaluation of all the terms in (18). Useful conversion is achieved by evaluating the strong wavelength dependence of the multiplying terms and scaling by a (weakly wavelength-dependent) comparison with a known scatterer. The important terms in (18) are now examined.

Synchrotron flux

Knowledge of the synchrotron-radiation flux $J_{in}(\lambda)$ is essential to the conversion to absolute units. Synchrotron sources can be sufficiently well characterized as emitters of electromagnetic radiation that the flux available, its wavelength dependence and its polarization can be calculated from first principles. Some sources have been treated as radiometric standards (Krumrey *et al.*, 1989), though such accuracy is not usually achievable. The divergence of electron-beam trajectories, their spatial spread and the presence of field variations over the bending region are relatively minor complications that can be allowed for if the source is single and incoherent. The flux available over a finite aperture at the experimental station and its polarization should therefore be available as part of the synchrotron experimental station support. Alternatively, it can be independently calculated using a program such as that given by Reid (1989). Laundy, Cummings, Pattison, Honkimäki & Sleight (1990) presented a comparison between absolute flux measurements and calculated flux measurements on the Daresbury wiggler line that show good general agreement, the differences being thought due to defects in the measured values. Related measurements on the radiation from a dipole magnet (at the same station used by the author) produced an excellent agreement between the observed and calculated

spectral profile (Laundy, Cummings & Pattison, 1991).

Quantities required to determine $J_{in}(\lambda)$ are the average electron-beam current in the synchrotron ring during measurement, the source-to-sample distance, the spread parameters of the source and the beam-aperture sizes. If the beam itself is accurately monitored by a detector that is linear with intensity and spatial size, then allowance can be made for (small) changes in intensity that occur with instability of the source. We have not done this. The absorption of windows in the beamline can also be easily included. For the calculation to be relevant, the position of the beam-defining slits relative to the axis of the radiation cone must be centred (or known) to within, say, 20% of the actual r.m.s. opening angle of the radiation. This will be larger than the point-source opening angle on account of the finite source size and spread. The extent to which the position of the centre of the radiation cone at the experimental station is stable in time and between successive fills of the machine should be determined from operations staff or, better, by measurement. Fig. 3 sets the requirements in perspective. The contours illustrate the percentage error in the integrated flux that will be made when beam shifts are ignored. The effect increases strongly at smaller wavelengths, as the radiation cone narrows. Owing to uncertainties in several of the parameters determining $J_{in}(\lambda)$, one would not expect a high absolute accuracy unless special care is taken, though the wavelength dependence should be relatively well represented.

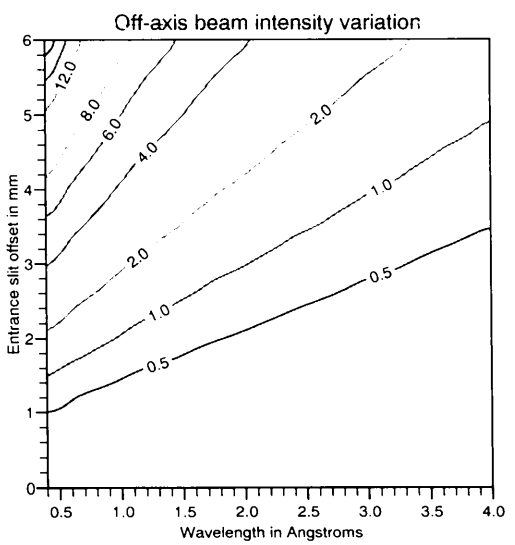

Fig. 3. Off-axis beam intensity variation. A slit 3 mm high and 79 m from a 2 GeV source defines the beam (angular equivalent 38 μrad). The slit is translated vertically from the centre of the radiation cone by up to 6 mm (1 mm = 12.7 μrad). The contours show the calculated percentage error in the received flux for a range of X-ray wavelengths if the shift is ignored. Flux integrations over the slit width include convolutions over the finite source size and divergence, with figures appropriate to the Daresbury 2 GeV source. The quantity plotted is $100\times(\text{Ratio}-1)$, where Ratio = flux(axial slit)/flux(shifted slit).

Absorption term

The structural crystallographer is not on the whole worried about the total absorption of the sample but about the absorption anisotropy, particularly for samples in the form of needles or plates. Even then, the absorption obtained by calculation or by an empirical method produces only a correction to the fitted structure. In contrast, for the absolute conversion of diffuse-scattering intensities, the total absorption term must be accurately evaluated.

For a crystal bathed in a uniform parallel incident beam, scattering through an angle 2θ, the absorption-related scattering contribution is

$$A(\theta, \varphi, \chi, \omega, \lambda) = n \int_V \exp[-\mu(l+l')]\,\mathrm{d}V, \qquad (19)$$

where l and l' are respectively the path lengths of incident and scattered beams to the illuminated volume element $\mathrm{d}V$ within the sample and n is the number of unit cells per unit volume,

$$n = N_A\rho/gW, \qquad (20)$$

where N_A is the Avogadro constant, ρ the material density, W the molecular weight and g the number of molecules per unit cell.

It is only practical to evaluate the absorption term under assumptions that are not mathematically precise; where possible, experimental conditions should be made to favour these asumptions. The path lengths l, l' are evaluated with the assumption that all scattered rays are parallel, as would be the case for a detector at infinity. The detector distance should therefore be as large as possible. [The finite size of the detector is accounted for by the convolution term D in (18).] The incident and scattered radiations are assumed to have the same attenuation coefficient μ. This is not quite valid for the Compton component of the scattering, the approximation being worse at large 2θ where the Compton energy shift is greatest. Finally, though the approximation of a uniform incident white beam is not strictly true, either, for the very small opening angles at short wavelengths, it becomes less important in this region of the spectrum because the absorption itself falls dramatically with decreasing wavelength.

The absorption integral of (19) must be calculated as a function of 2θ and sample orientation, since it is likely that the sample will be strongly absorbing for at least some of the wavelength range of interest. Indeed, the wavelength range may well cover the complete absorption regime, from light absorption at short wavelengths to strong absorption at longer wavelengths, making $A(\theta, \varphi, \chi, \omega, \lambda)$ a critical term

in (18) that can vary by several orders of magnitude across the spectrum. The simplest analytic absorption correction is found with the semi-infinite slab whose face is perpendicular to the scattering plane, the shape used by Harada *et al.* (1984) in their pioneering experiment. In this case,

$$A(\theta, \varphi, \chi, \omega, \lambda) = n/\mu[1+(\sin\alpha)/(\sin\beta)], \quad (21)$$

where α is the acute angle between the incident beam and the crystal surface and β is the acute angle between the detector direction and the crystal surface.

The extended-face slab has, however, several disadvantages: only reflection geometry can be used, significantly reducing the accessible range of scattering vectors **K**; only heavy-element materials have an adequate absorption coefficient at shorter wavelengths to justify the semi-infinite approximation for modest sample thicknesses; part of the emerging scattered beam can be well separated from the incident beam, thereby making the effective source of the diffuse scattering large and hence degrading the resolution of the experiment.

For a sample of any shape, at the longer wavelengths sampled by the energy-dispersive detector, the sample is almost certain to be highly absorbing. In these circumstances only small parts of the sample contribute to the scattered intensity and the calculation of the absorption by normal numerical means (such as Gaussian quadrature) becomes inaccurate. This inaccuracy arises because numerical methods divide the sample into lines of volume elements stretching across the sample; any density of elements sufficient to give an accurate answer when the contribution comes from small regions of the sample entails a division of the total volume into an excessive number of subvolumes for practical computation. Recourse has to be made to an analytic absorption calculation or under special circumstances of high symmetry a numerical evaluation must be formulated to overcome the difficulty.

The general analytic method of de Meulenaer & Tompa (1965) for a convex polyhedral crystal provides the basis for the evaluation of $A(\theta, \varphi, \chi, \omega, \lambda)$, provided the crystal is a well defined polyhedron. For diffuse-scattering measurements it is desirable that only the crystal is irradiated and not any of the crystal support, which can contaminate the spectrum with scattering of comparable strength. The scattered volume is therefore defined jointly by the crystal faces and the planes that define the incident beam above and below the scattering plane. If only a section of the crystal is irradiated, the geometry has to be further modified. In all cases, the absorption correction is calculated on the assumption that multiple scattering does not contribute significantly to the observed intensity.

In the work to be reported in paper II, a crystal was used in the form of a long rod extending through the beam. In any plane parallel to the scattering plane, the cross section of the crystal is therefore the same and hence the absorption integral the same. In these circumstances the planar analytic method of Howells (1950) can be employed, which is simpler though by no means trivial. We have also used cylindrical rods oriented perpendicular to the scattering plane. In this case the absorption is independent of the rotation angle of the sample.

At high absorptions only those parts of the crystal that are directly seen by both incident beam and detector contribute significantly to the scattering. The scattering volume involved, and hence the effective size of the sample, shrinks rapidly with increasing wavelength. When the departures of the real crystal shape from the modelled shape become comparable to the penetration depth of the radiation, the absorption calculation loses its validity. There are many possible causes for such departures. Taking 40 μm as an estimate of the modelling accuracy (sometimes one can do better, often worse), the corresponding linear absorption coefficient is 250 cm^{-1}. Table 1 shows the wavelengths at which the absorption coefficient has risen to this value for crystals of the elements at room temperature. In effect, it shows the

Table 1. *Estimate of the long-wavelength limit* (λ) *at which the penetration depth* $1/\mu$ *is* 40 μm *for crystals of the elements at room temperature*

Absorption coefficients were calculated from the parameters in *International Tables for X-ray Crystallography* (1983). Crystal densities were obtained from the *CRC Handbook of Chemistry and Physics* (1972), in which they are usually quoted at 293 K. For the element C, diamond is represented; for other elements with a range of allotropes, the chosen density is either that of the most common variant or the median.

Element	Wavelength (Å)	Element	Wavelength (Å)	Element	Wavelength (Å)
Li	14.859	Ge	0.630	Pr	0.634
Be	7.285	As	0.596	Nd	0.621
B	5.675	Se	0.621	Pm	0.604
C	3.936	Rb	1.738	Sm	0.577
N	6.472	Sr	0.721	Eu	0.646
Na	3.235	Y	0.564	Gd	0.548
Mg	2.432	Zr	0.494	Tb	0.530
Al	1.936	Nb	0.420	Dy	0.514
Si	1.879	Mo	0.385	Ho	0.500
P	1.789	Tc	0.361	Er	0.486
S	1.750	Ru	0.343	Tm	0.473
K	2.000	Rh	0.336	Yb	0.517
Ca	1.539	Pd	0.334	Lu	0.449
Sc	1.157	Ag	0.345	Hf	0.397
Ti	0.951	Cd	0.365	Ta	0.360
V	0.818	In	0.383	W	0.337
Cr	0.740	Sn	0.377	Re	0.322
Mn	0.707	Sb	0.385	Os	0.309
Fe	0.664	Te	0.747	Ir	0.305
Co	0.614	I	0.795	Pt	0.306
Ni	0.592	Cs	1.092	Au	0.313
Cu	0.572	Ba	0.852	Hg	0.352
Zn	0.601	La	0.679	Tl	0.365
Ga	0.625	Ce	0.646	Pb	0.365
				Bi	0.382

wavelength limit for reliable modelling of these crystal shapes. A given element clearly has a less limiting effect when it occurs in a compound.

At the wavelengths shown and at all longer wavelengths on the same side of the absorption edge, the effective scattering volume is small. It can be seen that high absorption is particularly damaging to the energy-dispersive technique once elements as heavy as the transition metals are reached. Either heavy elements should be present only dilutely in a compound or the energy-dispersive technique should be operated in the hardest X-ray wavelength range. It is for heavy-element materials that the extended-face geometry comes back into its own.

Absorption may also limit the radial resolution that can be achieved. If the lattice constant is large or the range of scattering vectors of interest is small, it is advantageous to scan at small 2θ. If the crystal absorbs significantly, however, the absorption increases strongly as 2θ becomes small, with a corresponding decrease in scattered-beam strength. This decrease in intensity can be sufficient to make measurements impractical at small 2θ, as is illustrated by representative numbers in Fig. 4. These were evaluated for a silicon cylinder of 1 mm radius, as detailed in the Fig. 4 caption. The changes in the absorption integral of (19) may not look spectacular because they are shown on a logarithmic scale. $\ln[A(\theta, \varphi, \chi, \omega, \lambda)] = 6$ represents an absorption factor of about 400 and hence a reduction in observed intensity by 400 from what it would have been if the absorption were negligible. If this number, for example, represented the practical upper limit of absorption, then Fig. 4 shows that measurements on the sample could not be made below

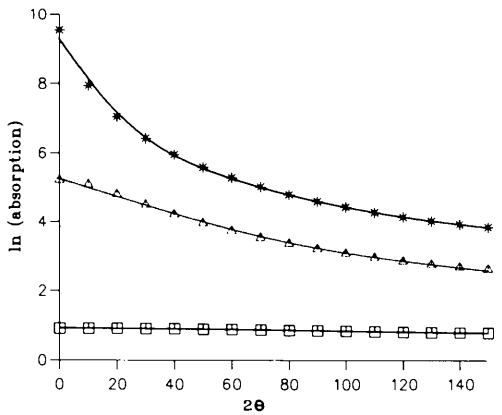

Fig. 4. The changing absorption contribution, from (19), with 2θ for a range of absorption coefficients. Note that $\ln[A(\theta, \varphi, \chi, \omega, \lambda)]$ is plotted since the changes are too large to show on a linear scale. The sample is a cylinder of silicon of radius 1 mm, oriented perpendicular to the scattering plane. □ Variation with low absorption ($\lambda = 0.5$ Å, $\mu = 5.6$ cm^{-1}); △ medium absorption ($\lambda = 1.0$ Å, $\mu = 40.3$ cm^{-1}); * high absorption ($\lambda = 1.5$ Å, $\mu = 130.6$ cm^{-1}).

$2\theta = 40°$ while retaining the wavelength range 0.5 to 1.5 Å.

Remaining terms

The effect of incident-beam cross fire, finite sample and detector sizes, and the sample mosaic spread on the resolution-function correction term D in (18) has been dealt with at some length by Reid (1981). For an energy-dispersive scattering configuration on a synchrotron-radiation station, all aspects of the experimental arrangement tend to keep these effects small and D correspondingly small. The largest influence on the resolution correction is likely to be the energy resolution of the detector which, through (16) and (17), results in a convolution of the scattering intensity with a Gaussian profile of standard deviation $\Delta_{\mathrm{HWHM}}(E)/1.167$. In the results presented in paper II, no deconvolution has been attempted.

The final term $\varepsilon(\lambda)$ can be estimated from the known behaviour of the detector and of absorption of air and windows in the path length. $\varepsilon(\lambda)$ includes not only the intrinsic photon-counting-efficiency variation but also the effects of uncorrected differential nonlinearity of the MCA, which affects the count recorded in each channel. However, the variation of $\varepsilon(\lambda)$ can also be measured by using the inherent redundancy of Laue geometry. The same scattering vector **K** may be measured at different wave vectors by changing 2θ and simultaneously rotating the crystal by θ about the main diffractometer axis. Alternatively, an amorphous sample may be used and the sample rotation ignored. Equation (10) shows that a feature in the converted spectrum that appears at a given d^* will be due to a wavelength that varies as $\sin\theta$. One strategy is to track a reference wavelength, for which $\varepsilon(\lambda)$ can be taken as unity, through the spectrum by a series of measurements at different θ. A second approach is to measure two spectra at angles of θ differing by a few degrees and deduce by interpolation and iteration the function $\partial\varepsilon/\partial\lambda$ from the ratio of the converted results at constant d^*. In either case, appeal has to be made to one calculated value. Of course, one or more values may be obtained for $\varepsilon(\lambda)$ from measurements on a standard scattering sample, whose absolute cross section is known at one or more values of d^*.

Concluding remarks

It is too early to say whether the potential advantages of the white-radiation technique outlined in the *Introduction* will lead to its widespread application. Much depends on the accuracy achieved for the conversion to absolute units by use of the principles discussed here. Much also depends on practical matters such as the satisfactory alignment of small samples on supports that do not themselves provide comparable diffuse scattering; on the control of

geometrical factors to obtain adequate resolution; on the avoidance of fluorescence that can saturate the present generation of energy-dispersive detectors and thereby swamp the diffuse scattering. The first and last of these points introduce significant extra difficulties with white radiation over the use of monochromatic X-rays or neutrons.

The most promising applications are with light-element materials, where the absorption of adequately sized samples is modest for wavelengths below 1 Å and their fluorescence above 2 Å is either beyond the energy response of the detector or can be readily blocked by a thin filter. Harada *et al.* (1984) have demonstrated that applications are also possible with heavy-element materials, where the *K* fluorescence is too hard to be excited and the *L* fluorescence can be tolerated. Paper II of this series will discuss results obtained using light elements.

The author would like to thank the Science and Engineering Research Council for grant support during the development of this subject; staff at the Daresbury Synchrotron Radiation Laboratory for their encouragement, particularly Phil Pattison (now developing facilities at ESRF); at Aberdeen University, John D. Pirie and Stephen D. Clackson for discussions during the practical development of the technique, which will be illustrated in paper II.

References

CRC Handbook of Chemistry and Physics (1972). Boca Raton, Florida: Chemical Rubber Co.

HARADA, J., IWATA, H. & OHSHIMA, K. (1984). *J. Appl. Cryst.* **17**, 1-6.

HASEGAWA, K., MOCHIKI, K., KOIKE, M., SATOW, Y., HASHIZUME, H. & IITAKA, Y. (1986). *Nucl. Instrum. Methods Phys. Res.* A**252**, 158-168.

HOWELLS, G. (1950). *Acta Cryst.* **3**, 366-369.

International Tables for X-ray Crystallography (1983). Vol. III, pp. 171-173. Birmingham: Kynoch Press. (Present distributor Kluwer Academic Publishers, Dordrecht.)

IWASAKI, H., MATSUO, Y., OHSHIMA, K. & HASHIMOTO, S. (1990). *J. Appl. Cryst.* **23**, 509-514.

IWASAKI, H., SASAKI, S., KISHIMOTO, S., HARADA, J., SAKATA, M., FUJII, Y., HAMAYA, N., HASHIMOTO, S., OHSHIMA, K. & OYANAGI, H. (1989). *Rev. Sci. Instrum.* **60**, 2406-2409.

JAGODZINSKI, H. (1987). *Prog. Cryst. Growth Charact. Mater.* **14**, 47-102.

KRUMREY, M., TEGELER, E. & ULM, G. (1989). *Rev. Sci. Instrum.* **60**, 2287-2290.

LAL, K. (1989). *Prog. Cryst. Growth Charact. Mater.* **18**, 227-266.

LAUNDY, D., CUMMINGS, S. & PATTISON, P. (1991). *Nucl. Instrum. Methods Phys. Res.* A**302**, 553-557.

LAUNDY, D., CUMMINGS, S., PATTISON, P., HONKIMÄKI, V. & SLEIGHT, J. (1990). Daresbury Annual Report 1989/1990, Appendix, p. 164. SERC Daresbury Laboratory, Warrington, England.

MAETA, H., LARSON, B. C., SJOREEN, T. P., THOMAS, D. K., OEN, O. S. & LEWIS, J. D. (1988). *Mater. Res. Soc. Symp. Proc.* **138**, 81-86.

MATSUBARA, E. & GEORGOPOULOS, P. (1985). *J. Appl. Cryst.* **18**, 377-383.

MEULENAER, J. DE & TOMPA, H. (1965). *Acta Cryst.* **19**, 1014-1018.

OSBORN, J. C. & WELBERRY, T. R. (1990). *J. Appl. Cryst.* **23**, 476-484.

REID, J. S. (1981). *Acta Cryst.* A**37**, 382-390.

REID, J. S. (1989). *Comput. Phys. Commun.* **54**, 307-314.

SHULTZ, H. (1982). *Current Topics in Materials Science*, Vol. 8, edited by E. KALDIS, pp. 277-379. Amsterdam: North-Holland.

WELBERRY, T. R. (1985). *Rep. Prog. Phys.* **48**, 1543-1593.

Acta Cryst. (1993). A**49**, 198-202

Ferroelectric Phase Transition in $Li_2Ge_7O_{15}$ Investigated by Mössbauer Diffraction

BY K. KREC AND W. STEINER

Institut für Angewandte und Technische Physik, Technische Universität Wien, Austria

AND M. WADA*

Synthetic Crystal Research Laboratory, Nagoya University, Nagoya, Japan

(*Received* 11 *October* 1991; *accepted* 24 *July* 1992)

Abstract

Mössbauer diffraction experiments were performed on a single crystal of lithium heptagermanate in the temperature range 250-350 K. The high energy resolution of resonant γ radiation was used to separate elastically and inelastically scattered components. A lattice expansion along **c** and a decrease of the intensity of the elastically scattered radiation (I_{Bragg}) connected with an increase of the intensity of the inelastically scattered radiation (I_{TDS}) are observed at the transition from the para- to the ferroelectric phase at 283.5 K. The experimentally determined maximum of I_{TDS}/I_{Bragg} appearing at the phase transition is much more pronounced in comparison with

* Present address: Department of Physics, Faculty of Liberal Arts, Shinshu University, Matsumoto, Japan.

0108-7673/93/010198-05$06.00